Chapter 2
Calibration and Validation of a Car Subframe Finite Element Model Using Frequency Responses

T.J.S. Abrahamsson, F. Bartholdsson, M. Hallqvist, K.H.A. Olsson, M. Olsson, and Å. Sällström

Abstract A finite element model of a car front subframe has been calibrated against test data. Stepped-sine testing has been used to give frequency response function estimates on an ensemble of seemingly identical subframes. Therefore, the deviation between test data and simulation results can be compared in a meaningful way by the outcome of model calibration and cross-validation. Emphasis has been put on the preparation of the test pieces for high fidelity testing and on bettering the chances of getting a calibration outcome that provides insight into the physical processes that govern the subframe dynamics. The front subframe model has more than 200,000 degrees-of-freedom and 17 model calibration parameters. The efficiency of the calibration procedure under these conditions is reported. To achieve efficiency, a calibration with a smooth deviation metric is used together with a damping equalization method that eliminates the need for matching of experimental and analytical eigenmodes. The method is combined with surrogate model frequency response evaluation based on model reduction for increased speed. The Matlab based open-domain software tool FEMcali that employs the Levenberg-Marquardt minimizer with randomized starts has been used for calibration and an unregularized Gauss-Newton minimizer has been used in the cross-validation.

Keywords FEM model calibration • FEM model validation • Large model calibration • Surrogate model • Damping equalization

2.1 Introduction

For car industry, as well as other advanced industry, it is important to shorten the development time and reduce cost for testing. This has increased the need for attribute predictions that are based on computational models with high credibility. Good modeling guidelines are essential to achieve trust in model predictions that are made prior to the availability of physical test objects. Such modeling guidelines should ideally be created based on the outcome of model correlation and validation studies made on test data from already existing components, subsystems or full systems. Since industry-size models tend to be very large, efficient methods for calibration, correlation and validation are needed in this process of increasing the model credibility. This paper concerns the calibration and validation of a subframe model for a Volvo V40 car. This part of the car was selected since it is represented by a reasonable large computational model and was believed to behave linearly under mild loading conditions. A Nastran model with 207,912 degrees-of-freedom is the target for calibration. The subframe and its physical location in the car is indicated in Fig. 2.1.

Many FEM calibration practices are based on modal analysis and modal comparisons. The accuracy of the FEM is determined by comparing modal data from test and analysis. The eigenfrequencies are compared directly, while the corresponding mode shapes are compared with various metrics. The metrics most often employed are based on the orthogonality and cross-orthogonality of the modes with respect to the mass distribution quantified by a FEM mass matrix, see [1]. A significant drawback of these metrics is the fact that there is not an explicit connection between the metric values and a corresponding deviation in a predicted response. Another drawback is that measurement noise, limited spatial resolution in the vibration sensing, and shortcomings that affect the test data quality and processed data often magnify the problems associated with closely spaced modes that produce a spurious coupling sensitivity between the test and FEM mode shapes. This sensitivity makes a modal orthogonality metric problematic for matching test and FEM mode shapes

T.J.S. Abrahamsson (✉)
Department of Applied Mechanics, Chalmers University of Technology, Hörsalsvägen 7A, S-41296 Göteborg, Sweden
e-mail: thomas.abrahamsson@chalmers.se

F. Bartholdsson • M. Hallqvist • K.H.A. Olsson • M. Olsson • Å. Sällström
Volvo Car Corporation, S-40531 Göteborg, Sweden

M. Mains (ed.), *Topics in Modal Analysis, Volume 10*, Conference Proceedings of the Society for Experimental Mechanics Series, DOI 10.1007/978-3-319-15251-6_2

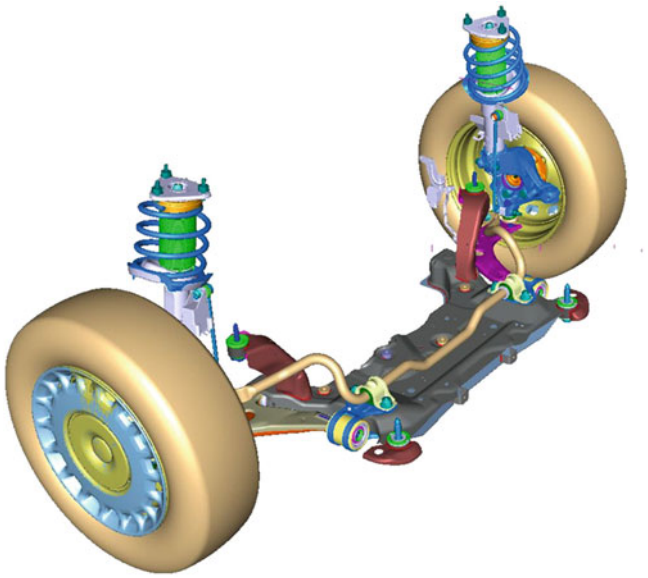

Fig. 2.1 Front subframe seen as placed in the car between the front wheels. The subframe is a vital part in the front wheel suspension and connects the suspension link arms to the car body and engine which makes it an important part regarding transmitted vibrations from road and engine

in the process of FEM calibration for systems with high modal density. Also, as the vibrational wavelengths approach the scale of structural geometry variations, the mode shapes become very sensitive to modelling errors and uncertainties [2–4]. Alternatively, modal approaches could be avoided by using frequency responses for FEM validation. Many researchers, e.g. Grafe [5], have studied model calibration using frequency domain data. The methods developed can loosely be categorized based on their criterion deviation metric as equation error methods or output error methods, or on their parameterization strategy, as direct matrix entity parameterization or physical property parameterization. In frequency domain equation error methods, such as described in [6–12], sensitivities of the FEM impedance matrix with respect to the design variables must be computed. One observed drawback of equation error approaches is that the comparably small number of responses measured in comparison to the large number of dofs in the FE model can produce non-smooth reduced impedance functions that have sharp peaks at the resonances that occur when the sensor dofs are fixed, see [6]. This can lead to a complicated calibration process in which a numerical calibration minimizer can easily be stuck in a local minimum. Output error methods on the other hand, such as described in References [13–18], attempt to minimize the difference between the measured data and the analytical prediction of that data. Balmès [13] minimized the least-squares or log-least-squares deviation in the frequency response functions. Herendeen et al. [14] presented a general multidisciplinary optimization framework for minimizing the deviation in any type of structural response. Dascotte and Strobbe [15] minimized the error in a frequency response function correlation metric that is based on the modal assurance criterion adapted to the frequency domain. The drawback of this approach is that the deviation metric, like many of the frequency response based deviation metrics in use [18], are not physically well motivated. There is no direct connection between a metric deviation and the deviation in the FEM prediction of responses due to loading. The advantage of the output approach is that no model dof reduction is necessary. However, these techniques require the minimization of an objective function that is non-linear in the parameters that can lead to minimizer convergence problems and a large computational effort.

Early developed FEM calibration strategies directly targeted the matrix entities of the FE mass and stiffness matrices by adjusting these to achieve best fit to test data. Recent papers, of more practical use to an engineer in the product development process, deal with model parameters that have clear physical interpretations, such as Youngs' moduli, material densities and thicknesses of shell-like parts. In a paper by Abrahamsson and Kammer [19] a discrete-frequency response based deviation metric was presented. It was shown that, together with a method for damping equalization that makes the calibration problem regularized, the metric gives good convergence properties for the calibration optimizer. The smoothness of the calibration metric was demonstrated to increase with increased system damping. In the damping equalization procedure the system damping can be arbitrarily set to any fictitious level for both the experimental data and the FEM. By assigning the same amount of modal damping to all system modes, modal correlation analysis for mapping of experimentally found damping to FEM damping can be avoided. By considering the FE coefficient matrices to be linear in the parameters around a linearization point, the reduced order model can be easily formed without expensive evaluation of the FEM equation as the model parameter settings vary as the iteration process proceeds to achieve the calibration minimum.

In this paper, the calibration and validation problem of a large scale FE model is treated by the method set out in [19]. The measurement procedure, involving tests of five seemingly identical subframes, is described. The outcome of the calibration, validation and cross-validation is reported and observations made during the process are discussed.

2.2 Theory

The theory presented in [19] is reiterated in condensed form here for reader convenience. We set out the theory from the FE representation of the linear time-invariant mechanical system as the set of ordinary differential equations

$$\boldsymbol{M}\ddot{\boldsymbol{q}} + \boldsymbol{V}\dot{\boldsymbol{q}} + \boldsymbol{K}\boldsymbol{q} = \boldsymbol{Q}(t) \tag{2.1}$$

with $M, V, K \in \Re^{n \times n}$ being the mass, viscous damping and stiffness matrices respectively. The displacement vector is here $\boldsymbol{q}$, and the dot notation is used for time differentiation. The vectorially associated loadings to $\boldsymbol{q}$ is $\boldsymbol{Q}$, for which just but a few entities are normally non-zero. These non-zero entities constitute the stimuli vector $u \in \Re^{n_u}$ from which the full load vector is given by the Boolean transformation matrix $\boldsymbol{P}_\mathrm{u}$ as $Q = P_u u$. It is assumed that only some mass and stiffness properties are subjected to calibration and therefore the FE problem is parameterized, with physical property parameters collected in data vector $P \in \Re^{n_p}$, such that the mass and stiffness matrices depend on these, i.e. $K = K(P)$ and $M = M(P)$. The physical parameter setting $\boldsymbol{P}$, with entities that can be of any order, is related to a normalized parameter vector $\boldsymbol{p}$ and some fixed non-zero nominal parameter setting $\boldsymbol{P}_0$ such that $P = P_0 \cdot (1 + p)$. The normalization of the parameters is made to better suit numerical minimizing schemes that often works better with scaled unknowns.

Using the dummy equation $I\ddot{q} - I\ddot{q} = 0$, the first-order differential equation counterpart to Eq. (2.1) can be formed as the state-space equations

$$\dot{\boldsymbol{x}} = \boldsymbol{A}\boldsymbol{x} + \boldsymbol{B}\boldsymbol{u} \quad \boldsymbol{y} = \boldsymbol{C}\boldsymbol{x} + \boldsymbol{D}\boldsymbol{u} \tag{2.2}$$

with the state vector $x^\mathrm{T} = \left\{ q^\mathrm{T} \; \dot{q}^\mathrm{T} \right\}$. It can easily be verified that the coefficient matrices $\boldsymbol{A}$ and $\boldsymbol{B}$ of Eq. (2.2) relate to the mass, damping and stiffness matrices such that

$$\boldsymbol{A} = \begin{bmatrix} 0 & \boldsymbol{I} \\ -\boldsymbol{M}^{-1}\boldsymbol{K} & -\boldsymbol{M}^{-1}\boldsymbol{V} \end{bmatrix} \quad \boldsymbol{B} = \begin{bmatrix} 0 \\ \boldsymbol{M}^{-1}\boldsymbol{P}_u \end{bmatrix} \tag{2.3}$$

and the matrices $\boldsymbol{C}$ and $\boldsymbol{D}$ are the appropriate matrices forming the system output $y \in \Re^{n_y}$ from linear combination of the states in $x \in \Re^{2n}$ and the stimuli in $\boldsymbol{u}$. Using the state-space representation (2.2), the system transfer function, relating the input to the output, can be expressed as

$$\boldsymbol{H}(\boldsymbol{p}) = \boldsymbol{C}(i\omega\boldsymbol{I} - \boldsymbol{A})^{-1}B + D \tag{2.4}$$

The transfer function $\boldsymbol{H}$ established from analytical FE data will here be denoted $\boldsymbol{H}^\mathrm{A}$. The experimentally determined system transfer function (denoted $\boldsymbol{H}^\mathrm{X}$) is often obtained from vibration testing and the use of signal processing and state-space system identification. The model calibration problem is thus about finding that parameter setting $p = p*$ (called the oracle parameter setting) that minimizes the deviation between $H^A(p)$ and H^X, i.e. $p* = argmin \left(f\left(H^A(p) - H^X \right) \right)$ with f being a calibration metric.

2.2.1 A Frequency Response Calibration Metric

A calibration scheme that uses a gradient based minimizer, needs to work with a smooth deviation metric for high likelihood of success. That is to obtain convergence in the search for parameter optimum from multiple start settings of the parameters. A well calibrated model should give high accuracy in simulation of test output quantities, and ideally predictions with high credibility of other output quantities not tested. In a frequency domain context, this often translates to that model which accurately captures the structural resonances and possibly also its anti-resonances. A metric that does not discriminate against deviations at frequencies where the structural response is small is the quadratic functional

$$\delta = \boldsymbol{\varepsilon}^H \boldsymbol{\varepsilon} / \boldsymbol{N} \tag{2.5}$$

which is called the square deviation (*SD*). In this the deviation vector $\boldsymbol{\varepsilon}$ is

$$\boldsymbol{\varepsilon}(\boldsymbol{p}) = \log_{10}\left(\text{vect}\left(\boldsymbol{H}^{\text{A}}(\boldsymbol{p})\right)./\text{vect}\left(\boldsymbol{H}^{\text{X}}\right)\right) \tag{2.6}$$

where the ./ operator denotes the element-by-element division and vect(.) is the vectorizing operation that makes all frequency response function elements of the $n_y \times n_u$ transfer function, at a dense set of n_f discrete frequencies used for evaluation, into an $n_y n_u n_f \times 1$ column vector. N is the number of elements of that vector.

Since finite element model calibration tends to be computationally demanding, calibration criteria that lead to computational efficiency are strongly of the essence. One such efficiency concern targets the sampling strategy for the discrete frequencies that are selected for frequency response function evaluation and the selection is based on the half-band width of the eigenmodes. The half-bandwidth $\Delta\omega_i$ of a damped structural resonance at frequency ω_i is given by $\Delta\omega_i = 2\zeta_i\omega_i$ with ζ_i being the relative modal damping of the i:th mode. One observes that the half-bandwidth increases linearly with increasing resonance frequency. It has been found to be a good frequency sampling strategy to utilize frequency steps that increase linearly with frequency to give a balanced contribution to the deviation metric from various system modes. Such sampling keeps the number of samples over one half-bandwidth constant over the range. That sampling strategy seems reasonable, provided that relative damping of all modes in the range is equal, which rarely happens for experimentally found eigenmodes. However, the damping can be equalized by a procedure that is described next.

2.2.2 Damping Equalization

A central issue for FRF based model calibration is that of model damping. Since in general, damping has been found to be very difficult to model using first principles, it is most often assigned a simple representation for modeling convenience. For modal damping modelling, the model's damping is usually set using the outcome of experimental modal analysis of test data from the structure under investigation. The modal dampings found in experiments are normally used for FE simulation without further attempts to understand their physical background. The nature of the damping mechanisms is normally such that the modal damping varies from mode to mode. That makes a mapping of experimentally obtained modal damping into modal damping of FE modes cumbersome. The difficulty arises since the mapping of modal damping relies on mode shape pairing, meaning that the same amount of modal damping should be assigned to modes that are in some sense similar by their deformation pattern. Such pairing is normally difficult, especially for systems with a high modal density. To overcome the problem of mode pairing, a method of damping equalization has been suggested [19]. The damping equalization is achieved by imposing the same modal damping on all experimentally found system modes by perturbation of a mathematical model of the experimental data found from system identification using raw frequency response function data $\boldsymbol{H}^X_{\text{raw}}$. The experimentally found system transfer function $\boldsymbol{H}^X_{\text{raw}}$ can then be represented by an identified state-space system $\dot{\boldsymbol{x}} = \boldsymbol{A}\boldsymbol{x} + \boldsymbol{B}\boldsymbol{u}$, $\boldsymbol{y} = \boldsymbol{C}\boldsymbol{x} + \boldsymbol{D}\boldsymbol{u}$ such that

$$\boldsymbol{H}^X_{\text{raw}} \approx \boldsymbol{C}(i\omega\boldsymbol{I} - \boldsymbol{A})^{-1}B + D \tag{2.7}$$

The experimental state-space system can be brought to diagonal form by a similarity transformation. Using the mode matrix $\boldsymbol{X}$, pertinent to the eigenvalue problem $\boldsymbol{A}\boldsymbol{X} = \boldsymbol{X}\boldsymbol{\Lambda}$, for transformation we have for the diagonal realization that

$$\boldsymbol{x} = \boldsymbol{X}\boldsymbol{z} \quad \dot{\boldsymbol{z}} = \overline{\boldsymbol{A}}\boldsymbol{z} + \boldsymbol{X}^{-1}\boldsymbol{B}\boldsymbol{u} \quad \boldsymbol{y} = \boldsymbol{C}\boldsymbol{X}\boldsymbol{z} + \boldsymbol{D}\boldsymbol{u} \tag{2.8}$$

with

$$\overline{\boldsymbol{A}} = \boldsymbol{X}^{-1}\boldsymbol{A}\boldsymbol{X} = \text{diag}(\lambda_i) \tag{2.9}$$

for which λ_i are the complex-valued system poles as given by the experimental data. For small damping, the relative modal damping ζ_i, obtained from these poles are

$$\zeta_i = -\Re(\lambda_i) / |\Im(\lambda_i)| \tag{2.10}$$

In the process of damping equalization, the real parts of the poles are perturbed such that the damping is made equal for all modes. The modal dampings are then set to a single fixed value ζ_0, i.e. $\zeta_i = \zeta_0 \ \ \forall i$. The effect of such damping equalization

is that the oscillatory imaginary part of the poles are preserved and the real damping part is modified such that the perturbed system poles $\tilde{\lambda_i}$ are now

$$\tilde{\lambda_i} = \Im(\lambda_i)(-\zeta_0 + \mathrm{i}), \quad \forall \Im(\lambda_i) > 0, \tilde{\lambda_i} = \Im(\lambda_i)(\zeta_0 + \mathrm{i}), \quad \forall \Im(\lambda_i) < 0 \tag{2.11}$$

and the modified state-space realization is then

$$\dot{z} = \tilde{\boldsymbol{A}} z + \boldsymbol{X}^{-1}\boldsymbol{B}\boldsymbol{u} \quad \boldsymbol{y} = \boldsymbol{C}\boldsymbol{X}z + \boldsymbol{D}\boldsymbol{u} \tag{2.12}$$

with $\tilde{\boldsymbol{A}} = \mathrm{diag}\left(\tilde{\lambda}_i\right)$. This in turn gives us a modified transfer function for the experimental model, such that the transfer function used for calibration with damping equalization is

$$\boldsymbol{H}^X \approx \boldsymbol{C}\boldsymbol{X}\left(i\omega\boldsymbol{I} - \tilde{\boldsymbol{A}}\right)^{-1}\boldsymbol{X}^{-1}B + DE \tag{2.13}$$

At this stage it should be obvious that the application of a system identification procedure on the raw test data $\boldsymbol{H}^X_{\mathrm{raw}}$ has led us to a mathematical model which we can evaluate for any frequency. We are also able to make fictitious modifications of the system under test. A particularly useful such modification is that we can adjust the system damping level, leaving stiffness and inertia properties intact, such that all system modal damping are set equal. The model calibration of the FE model can then be made towards this fictitious experimental model for calibration of parameters that relate to mass and stiffness only.

For the FE based system representation, the modal damping allows for a simple representation. For a system with given mass and stiffness matrices $\boldsymbol{M}$ and $\boldsymbol{K}$ we have the viscous damping matrix $\boldsymbol{V}$ to be [20]

$$\boldsymbol{V} = \boldsymbol{M}\boldsymbol{X}\,\mathrm{diag}\,(1/m_i)\,\mathrm{diag}\,(2\zeta_0 m_i \omega_i)\,\mathrm{diag}\,(1/m_i)\,\boldsymbol{X}^{\mathrm{T}}\boldsymbol{M} \tag{2.14}$$

with eigenfrequencies ω_i, modal masses m_i, and the modal matrix $\boldsymbol{X}$ given by the undamped system's eigenvalue problem

$$\boldsymbol{K}\boldsymbol{X} = \boldsymbol{M}\boldsymbol{X}\,\mathrm{diag}\left(\omega_i^2\right) \quad \mathrm{diag}\,(m_i) = \boldsymbol{X}^{\mathrm{T}}\boldsymbol{M}\boldsymbol{X} \tag{2.15}$$

In a calibration procedure we are then able to search for the mass and stiffness related parameters $\boldsymbol{p}$ of the FE model $\{K(p), M(p)\}$ that render the transfer function $\boldsymbol{H}^{\mathrm{A}}$ given by Eq. (2.4) and that let the criterion function of Eq. (2.5) to be minimal. The discrete frequencies used to evaluate Eq. (2.5) do not have to match the discrete frequencies used in testing. After a successful calibration, the FE model is in better agreement with test data. The eigenmodes from test and analysis are therefore normally well suited for mode-pair matching by correlation analysis. After such matching, the modal damping found in the experiment can easily be mapped to the finite element model's viscous damping matrix using Eq. (2.14).

2.2.3 Surrogate Modeling

To be practical, an FRF based model calibration requires rapid calculations of the frequency responses of the model as the parameter settings change in the iterative search for minimum deviation to test data. For big models this is undoable without model reduction. To obtain efficiency, a modal reduction scheme is here applied to create a surrogate model used by the calibration procedure. The eigenmodes of the corresponding undamped system at the nominal parameter configuration, belonging to all eigenvalues in a frequency range that significantly overlaps the frequency range of interest are then used for reduction. Let that range be $\omega = \left[\omega_{\mathrm{low}}, \omega_{\mathrm{high}}\right]$. To save computational effort, that reduction basis is kept constant within one full calibration cycle and thus not modified as the parameter settings vary during minimization procedure iterations. Let the eigenvalue problem formulated at the nominal parameter setting $\boldsymbol{p}_0$ be

$$\boldsymbol{K}(\boldsymbol{p}_0)\,\boldsymbol{T} = \boldsymbol{M}(\boldsymbol{p}_0)\,\boldsymbol{T}\,\boldsymbol{\Omega} \quad \boldsymbol{\Omega} = \mathrm{diag}\left(\omega_i^2\right)\ \forall \boldsymbol{\omega} = \left[\omega_{\mathrm{low}}, \omega_{\mathrm{high}}\right] \tag{2.16}$$

Then the mass and stiffness matrices at any parameter setting $\boldsymbol{p}$ of the reduced model are

$$\overline{\boldsymbol{M}}(\boldsymbol{p}) = \boldsymbol{T}^{\mathrm{T}}\boldsymbol{M}(\boldsymbol{p})\,\boldsymbol{T}\ \ \overline{\boldsymbol{K}}(\boldsymbol{p}) = \boldsymbol{T}^{\mathrm{T}}\boldsymbol{K}(\boldsymbol{p})\,\boldsymbol{T} \tag{2.17}$$

and, in particular at the nominal configuration

$$\overline{\boldsymbol{M}}_0 = \boldsymbol{T}^{\mathrm{T}} \boldsymbol{M}\left(\boldsymbol{p}_0\right) \boldsymbol{T} \;\; \overline{\boldsymbol{K}}_0 = \boldsymbol{T}^{\mathrm{T}} \boldsymbol{K}\left(\boldsymbol{p}_0\right) \boldsymbol{T} \tag{2.18}$$

We introduce the gradients of the reduced mass and stiffness matrices

$$\overline{\boldsymbol{M}}_{,j} = \boldsymbol{T}^{\mathrm{T}} \left(d\boldsymbol{M}/dp_j \Big|_{\boldsymbol{p}=\boldsymbol{p}_0} \right) \boldsymbol{T} \text{ and } \overline{\boldsymbol{K}}_{,j} = \boldsymbol{T}^{\mathrm{T}} \left(d\boldsymbol{K}/dp_j \Big|_{\boldsymbol{p}=\boldsymbol{p}_0} \right) \boldsymbol{T} \tag{2.19}$$

with respect to the *j*:th calibration parameter and note in particular that these may be computed without new eigensolutions since the reduction basis is kept invariant. A reduced order surrogate model that is linear in the parameters is taken as the first order expansion of the Taylor series of $\tilde{\boldsymbol{M}}$ and $\tilde{\boldsymbol{K}}$ about $\boldsymbol{p}_0$ as

$$\tilde{\boldsymbol{M}}(p) = \overline{\boldsymbol{M}}_0 + \sum\nolimits_{j=1}^{n_p} \left(\boldsymbol{p}_j - \boldsymbol{p}_{j,0}\right) \overline{\boldsymbol{M}}_{,j} \;\; \tilde{\boldsymbol{K}}(p) = \overline{\boldsymbol{K}}_0 + \sum\nolimits_{j=1}^{n_p} \left(\boldsymbol{p}_j - \boldsymbol{p}_{j,0}\right) \overline{\boldsymbol{K}}_{,j} \tag{2.20}$$

with $\boldsymbol{p}_{\mathrm{j},0}$ being the j:th parameter at the nominal setting. It can be observed that the surrogate model approximation error is likely to increase with parameter variation from $\boldsymbol{p}_0$ for two reasons. The first reason is that the reduction basis $\boldsymbol{T}$ is kept fixed and the second is that the $\{M(p), K(p)\}$ model itself is not necessarily linear in the parameters. One also notes that, once the reduced order model and its gradients are established from the full size FE mode, no further evaluation of the FE model is required. That leads to fast computations. With the state transformation $\boldsymbol{x} = \boldsymbol{T}\boldsymbol{\xi}$, the reduced order surrogate model fits well into the state-space setting of the system transfer function as given by Eq. (2.4). The corresponding state-space model matrices are

$$\boldsymbol{A} = \begin{bmatrix} 0 & \boldsymbol{I} \\ -\tilde{\boldsymbol{M}}^{-1}\tilde{\boldsymbol{K}} & -\tilde{\boldsymbol{M}}^{-1}\tilde{\boldsymbol{V}} \end{bmatrix} \boldsymbol{B} = \begin{bmatrix} 0 \\ \tilde{\boldsymbol{M}}^{-1}\boldsymbol{T}^{\mathrm{T}}\boldsymbol{P}_{\boldsymbol{u}} \end{bmatrix} \tag{2.21}$$

with the reduced viscous damping matrix $\tilde{\mathbf{v}}$ formed in analogy with Eq. (2.14). With such reduced order surrogate model the frequency response calculations for various parameter settings needed during the calibration minimization procedure can be made very efficiently.

2.2.4 Validation and Cross-Validation

For validation and cross-validation purposes we calculate the model deviation to test data that has not been used for calibration. We establish the validation deviation vector $\boldsymbol{\gamma}$ as

$$\boldsymbol{\gamma}\left(\boldsymbol{p}\right) = \log_{10}\left(\mathrm{vect}\left(\boldsymbol{H}^{\mathrm{A}}\left(\boldsymbol{p}\right)\right) ./ \mathrm{vect}\left(\boldsymbol{H}^{X}_{\mathbf{raw}}\right)\right) \tag{2.22}$$

in analogy with the calibration metric $\boldsymbol{\varepsilon}$ of Eq. (2.6), but here the transfer function relate to other frequencies or transfer function paths than were used for calibration. Also, the test data are taken as the raw test data and not the data computed from an identified state-space model. We also introduce the square deviation as a validation metric as

$$SD = \boldsymbol{\gamma}^{H}\boldsymbol{\gamma}/N \tag{2.23}$$

in which N is the number of data, i.e. the number of elements of the vector $\boldsymbol{\gamma}$. For a validated model we demand that the square deviation becomes smaller after calibration than before, and also that it becomes smaller than a specific target $\widehat{SD}$ that is established in line with the intended use of the model, i.e.

$$SD\left(\boldsymbol{p}^*\right) < SD\left(\boldsymbol{p}_0\right) \text{ and } SD\left(\boldsymbol{p}^*\right) < \widehat{SD} \tag{2.24}$$

For cross-validation we do statistics on the square deviation to establish the mean squared deviation (often called the residual squared error, *RSE*) and statistics on the calibration parameters after several calibrations in which various parts of the data has been used for repeated calibrations and the rest of the data used for establishing the square deviation. Since the repeated calibration result in varying parameter estimates, the statistics of the calibration outcomes is clearly of strong interest.

2.3 Calibration and Validation of the Subframe Model

The subframe FE model to be calibrated and validated is described first. A discussion on the testing, including considerations made after a pre-test, is made thereafter. The section concludes with results of the calibration, validation and cross-validation.

2.3.1 Finite Element Model and Its Parameterization

The subframe model is a Nastran FE model that consists of 39,978 nodes and 41,509 elements. Of these 35,254 are plate elements, 900 are solid elements, 1,782 are bar elements and 3,573 are rigid elements. The model was updated prior to calibration from a preliminary design CAD status to the best-of-knowledge-status of the subframe parts as they leave the production line. The density of the FE model parts were scaled to reflect the true weight of one subframe weighted on a high precision scale to be 16.985 kg. The nominal FE model indicates 18 elastic modes in free-free conditions below 800 Hz. The model and the first seven elastic modes are shown in Fig. 2.2. Seventeen parameters were selected for calibration. These were

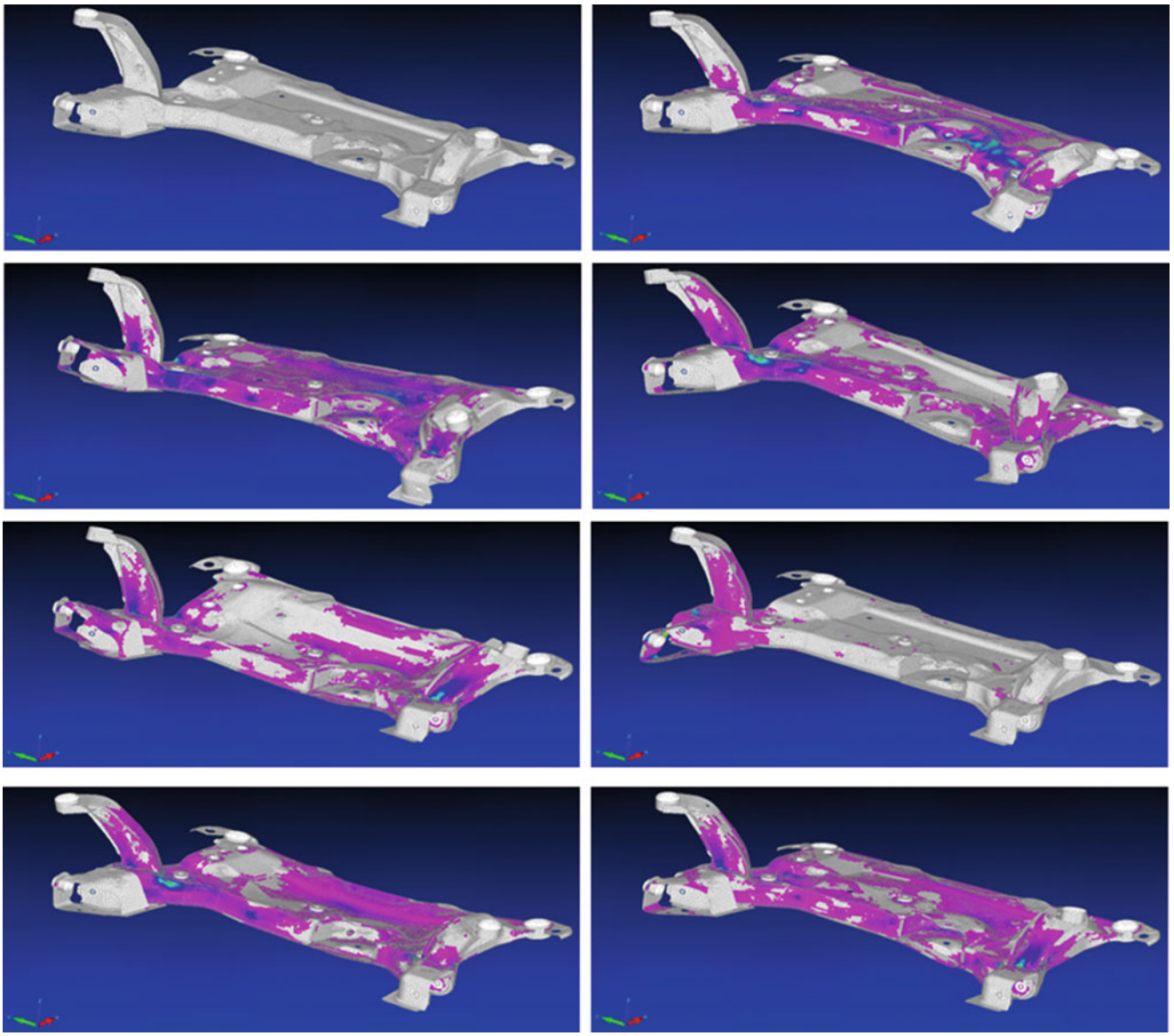

Fig. 2.2 Undeformed FE model (*upper left*) and seven flexible body modes in frequency range of calibration at 129, 174, 222, 266, 307, 348, 358 Hz. Eigenfrequencies are before calibration. The contour plots indicate regions of high strain (*blue/cyan/yellow*) and low strain (*magenta*)

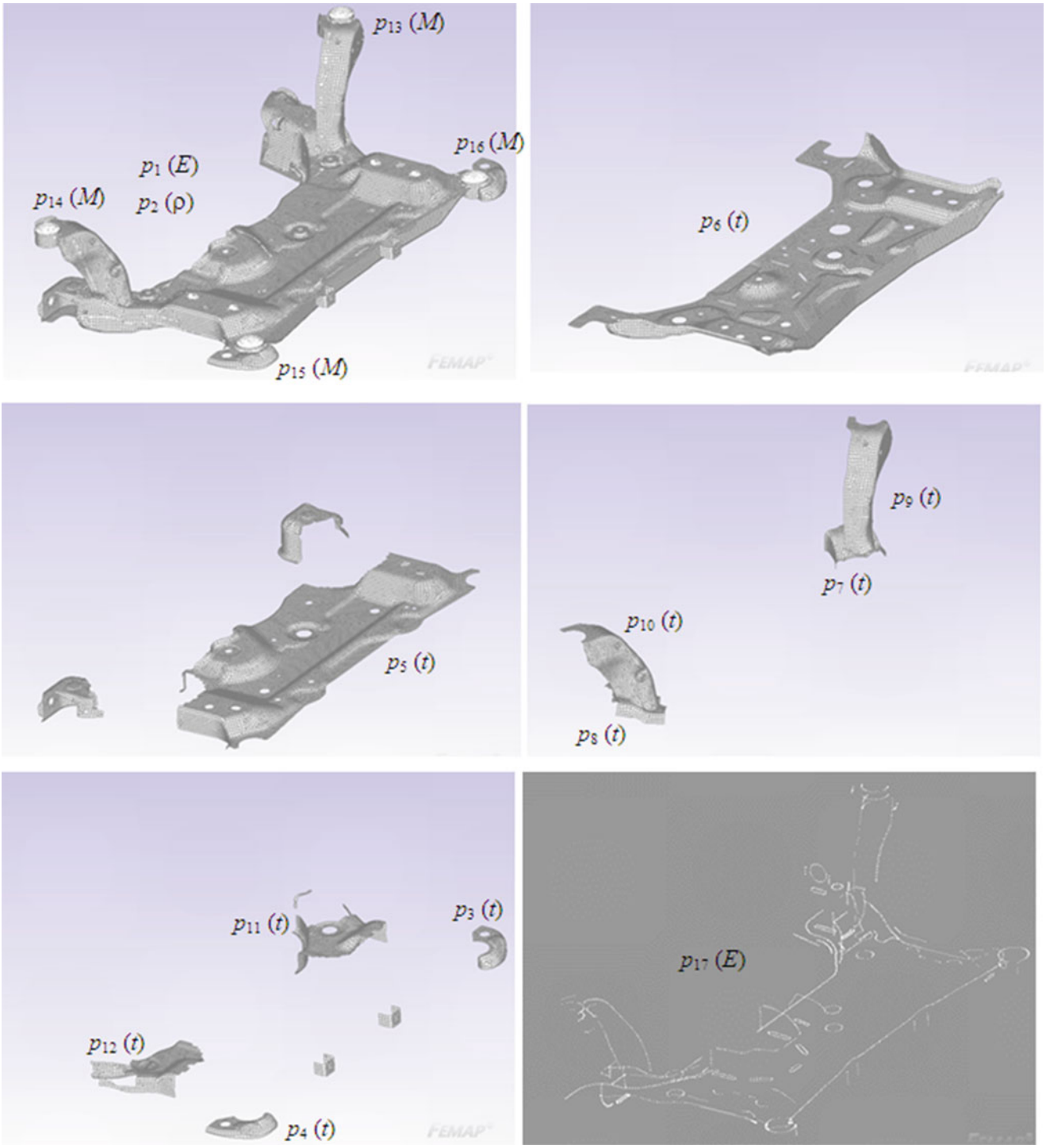

Fig. 2.3 Subframe domains affected by the parameters. *Top left*: parameters 1 and 2 (p_1 and p_2) are Youngs' modulus and density of overall subframe bulk material (steel). Four bushing masses are represented by parameters p_{13} through p_{16}. *Top right*: p_6 is thickness of bottom plate. *Mid left*: p_5 is thickness of top plate. *Mid right*: p_9 and p_{10} are thicknesses of LHS and RHS arms, and p_7 and p_8 are thicknesses of their base plates. *Bottom left*: parameters p_3, p_4, p_{11} and p_{12} represent thicknesses of various smaller parts of subframe. *Bottom right*: p_{17} is parameter representing elasticity (Youngs' modulus) of the welds

related to material stiffness and density, plate thickness, bushing masses and weld elasticity. The parameters are specified in Fig. 2.3. Many parameters, in particular the thickness parameters, can be seen as modeling placeholders for other physical properties such as geometry and thickness variations that results from the sheet metal forming of the various subframe parts.

2.3.2 Test Procedure and System Identification

Prior to testing, the accelerometer layout was decided based on the Effective Independence pretest planning scheme [21] targeting the first 20 elastic modes. A set of 20 single-axis accelerometers was used and two shaker locations used in two repeated SIMO tests between which the position of the shaker was moved. Data from one such SIMO test were used in this work. The shaker configurations were such that the actuation forces were collocated and co-oriented with accelerometers, see Fig. 2.4. A stepped-sine procedure was used with 1 N load magnitude and frequency steps in the range of a few tenths of a Hertz. Low-weight IEPE sensors, 0.5 g PCB Piezotronic type 352C22, were used to measure the accelerations and a Brüel&Kjær force sensor (type 8203 with IEPE converter 2647B) was used to measure the excitation force. The sensor layout is shown in Fig. 2.4. A significant effort was put on isolating the subframe test-pieces from the surrounding with a flexible supporting system. Two doubled very thin fishing lines (0.16 mm diameter and 1.8 m long), ending in a locking ring (see Fig. 2.4) at existing bolt holes on the subframe at one end and at flexible bungee cords at the fixture end resulted in a supporting system that gave six quasi-rigid body modes all below 4 Hz.

Five subframe units were tested in total. The test results separated the subframes into two groups with very similar results within each group, with two subframes in on group and three subframes in the other. A close inspection revealed that while two subframes had a clearly visible air gap between two particular sheet metal parts, the same air gap was closed and the sheet metal parts in tight contact for the other three subframes. The air gaps were all within production tolerances, but the impact it had on test data differences came as a surprise. Its impact was later examined by a FE analysis which confirmed the observation.

The data collection resulted in 20×2 frequency response function matrices of the five subframes. A system identification was made on a SIMO subset of data from one subframe using the N4SID state-space sub-space system identification method as implemented in the System Identification toolbox v9.0 in Matlab. Test data from 100 to 550 Hz were used to identify a model of state order 44 using SIMO data from shaking at point #17 (see Fig. 2.4 for its location). Frequency response function data up to 400 Hz from shaking at this point and a selection of 11 responses (accelerometers 1, 5, 7, 10, 12, 13, 14, 15, 18, 19 and 20) were used for calibration of the model. Data from the remaining 9 responses were used for a hold-out model validation.

2.3.3 Calibration and Validation Results

For the calibration and validation, test data in the frequency range 100–400 Hz have been used. The calibration and cross-validation were made using 11 transfer functions resulting from the SIMO testing with shaking at accelerometer #17. The remaining nine transfer functions obtained from the SIMO shaking at the same location were used for standard (hold-out) validation. The calibration was made using a damping equalization at 1 % relative damping and discrete frequency evaluations at a density of three samples per half-bandwidth. This relatively strong damping was set to regularize the calibration metric. Typical damping values for the identified modes below 400 Hz were in the order of 0.1 %. The calibration minimization was started from 20 randomized parameter settings in addition to the start from the nominal parameter setting.

The calibration resulted in a reduction of the square deviation for the calibration data from 1.748 to 1.156[−], thus a reduction by 33 %. The square deviation for validation data was reduced from 1.654 to 1.247[−], thus a reduction by 25 %. The cross-validation was done using 20 Monte Carlo realizations. In each such realization the data were split at random in two sets of equal size. While one set was used for calibration the other was used for calculation of the squared deviation. The *RSE* was calculated to be 1.036[−].

Resulting data for the calibration parameters are shown in Table 2.1. For the calibrated FE model, the mapping of experimentally found modal damping could be mapped to FE modes by mode correlation analysis. After such mapping, the FE model was used to synthesize frequency response functions corresponding to the experimental ditto. Typical frequency response functions from the calibration set are compared in Fig. 2.5. The comparison is made for the ensemble of tested subframes that showed similar behavior and for the FE model before and after calibration. Typical frequency response functions from the validation set are compared in Fig. 2.6.

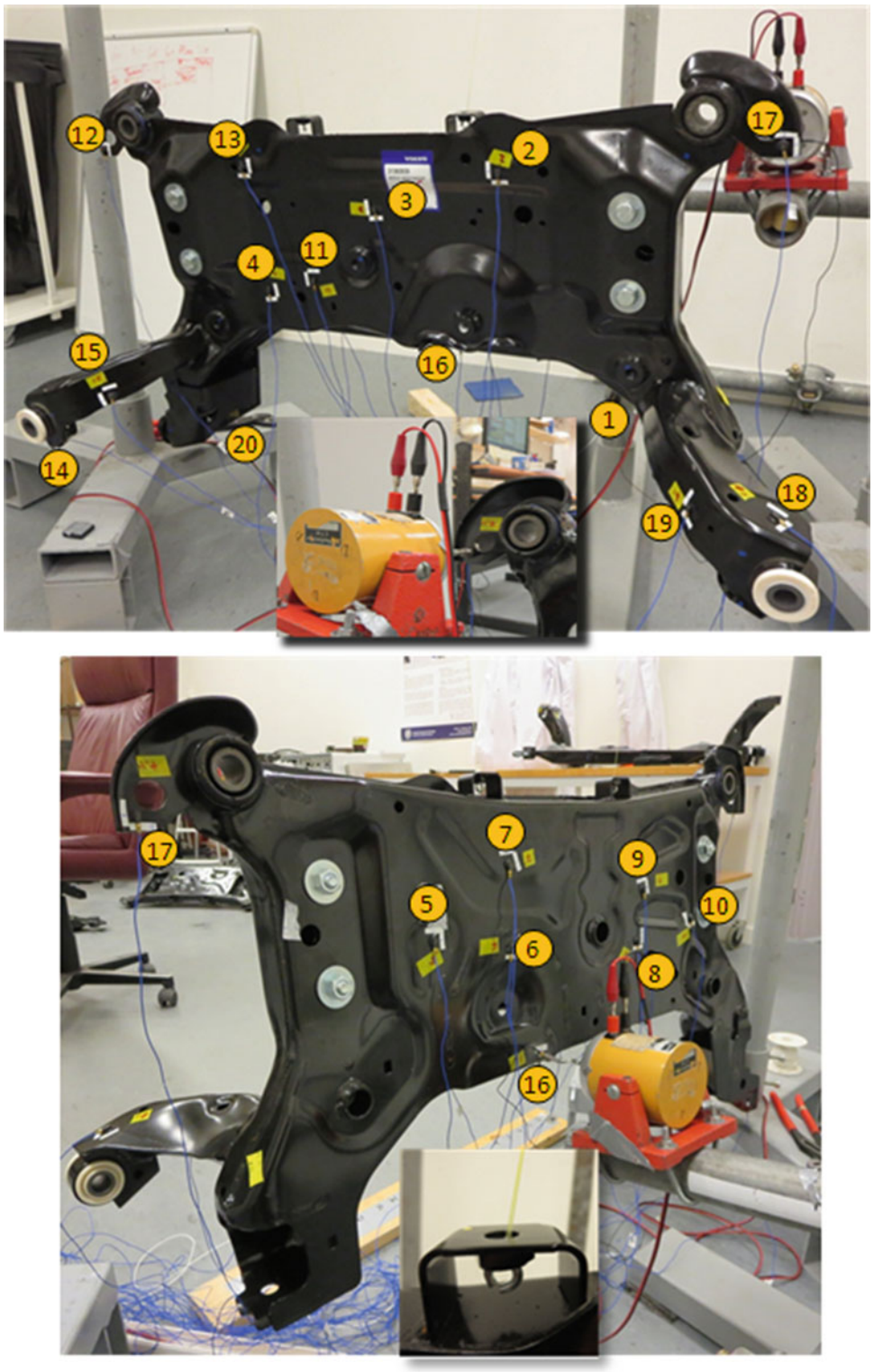

Fig. 2.4 Subframe from two different views. *Top view* shows position of 14 accelerometers visible from this viewpoint. The insert shows the position of the shaker with 5 mm long stinger and force sensor that sits just opposite of accelerometer #17 in one shaker configuration. *Bottom view* shows opposite side of subframe with position of other six accelerometers plus the two (16 and 17) that are at locations of shaker positions. Shaker is just opposite accelerometer #16 in *bottom view*. *Bottom insert* shows the supporting doubled fishing line that is threaded through a locking ring

2.3.4 Computational Efficiency

The calibration was made from 20 random starts and from the nominal parameter setting. The randomized starts were obtained from a latin hypercube sampling scheme. The calculations were made in 8 min 2 s to establish the nominal FE model, form the reduction basis and calculate the surrogate model gradients by parallel computation. It took 58 s to do the

Table 2.1 Parameter statistics with nominal and calibrated values. Mean values and coefficient of variation (CV) from cross-validation

#	Parameter	Nominal setting	Calibrated setting	Mean	CV [%]
1	E main	210 GPa	217	217	0.04
2	ρ main	7,850 kg/m^3	7, 750	7, 750	0.0
3	t bracket RHS	2.5 mm	2.46	2.46	0.012
4	t bracket LHS	2.5 mm	2.52	2.53	0.018
5	t top skin	2.3 mm	2.21	2.20	0.072
6	t bottom skin	2.0 mm	1.96	1.95	0.151
7	t arm base RHS	2.3 mm	2.33	2.33	0.0
8	t arm base LHS	2.3 mm	2.22	2.22	0.0
9	t arm RHS	3.0 mm	3.02	3.02	0.060
10	t arm LHS	3.0 mm	3.04	3.05	0.071
11	t arm extended base RHS	2.3 mm	2.46	2.47	0.080
12	t arm extended base LHS	2.3 mm	2.35	2.35	0.036
13	Bushing mass M_1	0.136 kg	0.135	0.135	0.031
14	Bushing mass M_2	0.136 kg	0.138	0.138	0.030
15	Bushing mass M_3	0.215 kg	0.211	0.211	0.015
16	Bushing mass M_4	0.215 kg	0.227	0.227	0.023
17	Weld elasticity E	210 GPa	207	207	0.0

evaluation of 200 latin hypercube sampling evaluations in parallel and it took 5 min 50 s to do the calibration calculations in parallel. This result in 14 min 50 s total calculation time for the calibration. The hold-out validation took 5 min 16 s which includes the calculation of an updated surrogate model at the calibration parameter configuration and a mapping of the experimentally found modal dampings. The cross-validation with 10 Monte Carlo samples took 17 min 8 s with the majority of time spent on the 10 recalibrations from the calibrated parameter configuration as a starting guess. The overall time spent by the computer was 37 min 14 s.

The calculations were made in Matlab on a desktop PC with an AMD FX-8350 eight-core CPU running at 4 GHz and having 32 GB memory. The FE model was established in MSC.Nastran. A DMAP alter was introduced in a SOL103 solution sequence to get Nastran to release mass and stiffness matrix data as soon as it had been created.

2.4 Concluding Remarks

The work reported here is a continuation of the work reported in [22]. The results that were reported in [22] led to further physical insight that was used to modify the subframe FEM into one that is in better agreement with test observations. The starting point for this work was that refined FE model.

Although not fully reported here, a significant effort was made to get proper test data. The test campaign started with five subframe units. Preliminary testing showed a non-linear behavior also at low excitation levels. Two units were disassembled and the cause of the nonlinearity was found to be internal parts that were connected by loose joints. These parts are tightly bounded in the operation condition in the car by bolt connections. A surrogate of the true bolt connections was introduced by four bolts to the remaining three subframes which are visible in Fig. 2.4 as the blank bolt heads. When properly mounted, these surrogate bolts significantly diminished the nonlinear behavior.

It has been demonstrated that the calibration of a large-scale FE model is feasible and with reasonable outcome. With respect to validation data, the model has been made more trustworthy and the square deviation in the validation data set has decreased by about 25 %. The full calibration and validation calculations can be made in little more than ½ hour on a modern desktop computer anno 2014.

Since some FE model parameters are used as surrogates for the true physics, still some interpretation of the calibration results is needed to get more insight into the true physical phenomena that cause the deviation between analysis and test. However, it is strongly believed that such interpretation of the calibration results is of the essence for gaining physical insight to the benefit of future modeling.

The calibration and validation has been made using the open source Matlab application FEMcali, which can be downloaded from Mathwork's web at www.mathworks.com.

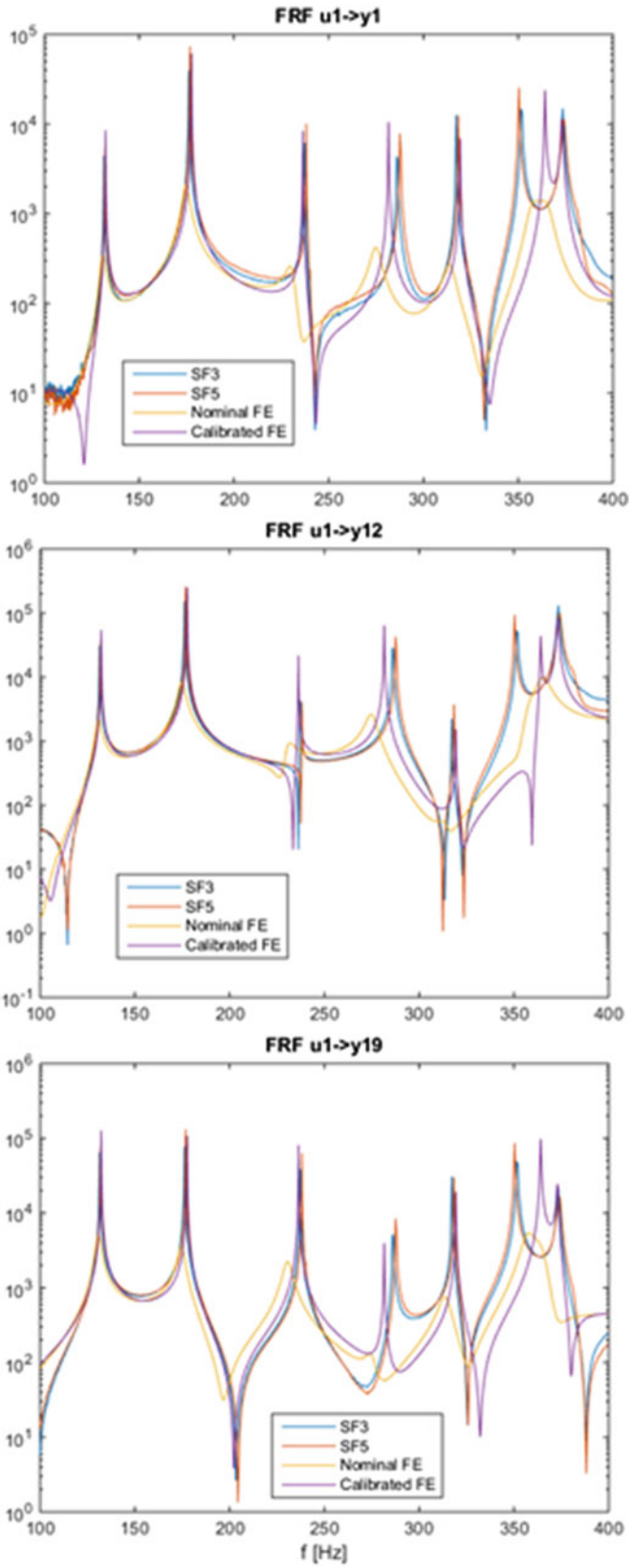

Fig. 2.5 Typical frequency response functions from calibration set. Note that the nominal FE model damping was set to 1 % while the calibrated FE model has mapped damping from test

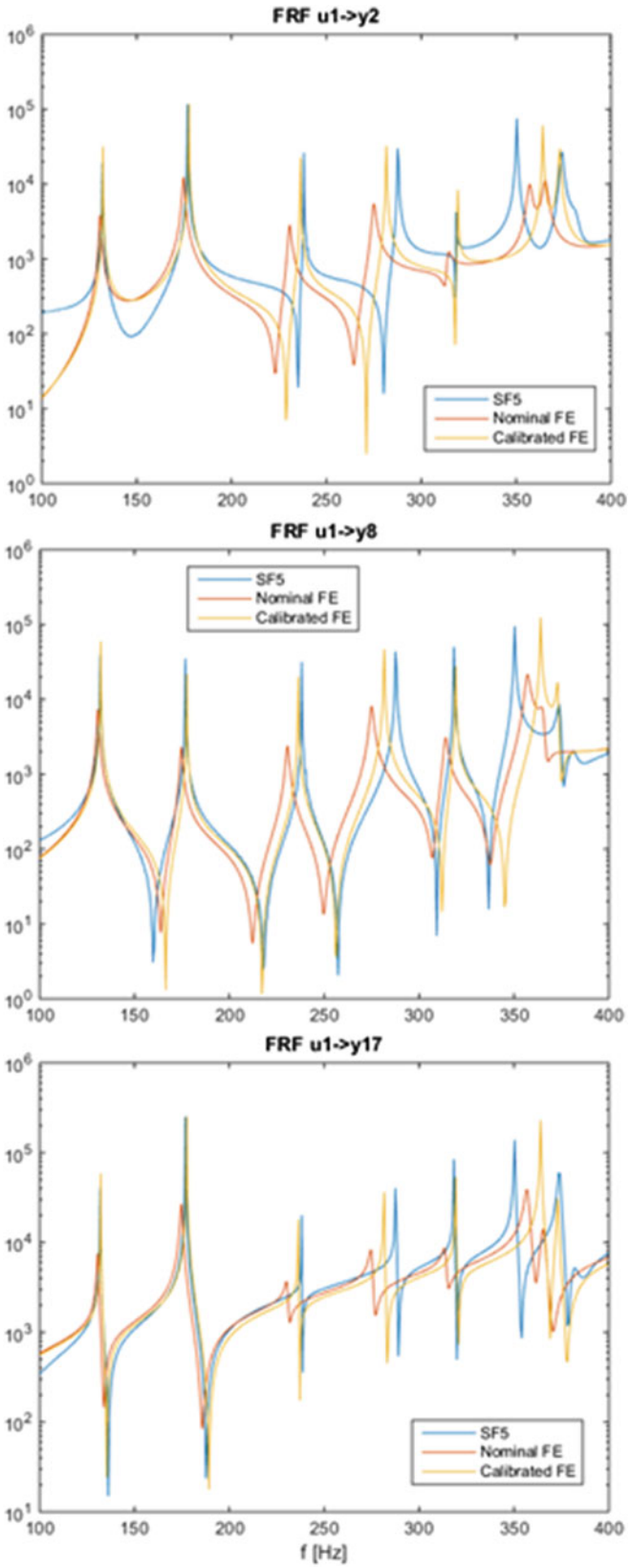

Fig. 2.6 Typical frequency response functions from validation set

References

1. Hasselman TK, Coppolino RN, Zimmerman DC (2000) Criteria for modeling accuracy – a state-of-the-practice survey. In: Proceedings of IMAC XIIX, San Antonio
2. Sarkar A, Ghanem R (2002) Mid-frequency structural dynamics with parameter uncertainty. Comput Meth Appl Mech Eng 191:5499–5513
3. Sarkar A, Ghanem R (2003) A substructure approach for the midfrequency vibration of stochastic systems. J Acoust Soc Am 113(4):1922–1934
4. Hasselman T, Anderson M, Lai YC (1998) Linking FEA and SEA by principal component analysis. In: Proceedings of IMAC XVI, Santa Barbara
5. Grafe H (1998) Model updating of large structural dynamics models using measured response functions. Ph.D. thesis, Imperial College, London
6. Larsson P-O, Sas P (1992) Model updating based on forced vibration testing using numerically stable formulations. In: Proceedings of IMAC X, San Diego
7. Gordis JH (1993) Spatial, frequency domain updating of linear structural dynamic models. In: Proceedings of 34th AIAA/ASME/ASCE/AHS/ASC structures, structural dynamics, and materials conference
8. Schultz MJ, Pai PF, Abdelnaser AS (1996) Frequency response function assignment technique for structural damage identification. In: Proceedings of IMAC XIV, Dearborn
9. Rad SZ (1997) Methods for updating numerical models in structural dynamics. Ph.D. thesis, University of London, London
10. Thyagarajan SK, Schultz MJ, Pai PF (1998) Detecting structural damage using frequency response functions. J Sound Vib 210:162–170
11. Zimmerman DC, Simmermacher T, Kaouk M (1995) Structural damage detection using frequency response functions. In: Proceedings of IMAC XIII, Nashville
12. Nauerz A, Fritzen C (2001) Model based damage identification using output spectral densities. ASME J Dyn Syst Meas Control 123:691–698
13. Balmès E (1993) A finite element updating procedure using frequency response functions – application to the MIT/SERC interferometer testbed. In: Proceedings of IMAC XI, Kissimmee
14. Herendeen DL, Woo L, Hasselman TK, Zimmerman DC (1998) Analysis-test correlation and model updating of dynamic systems using MDO software tools. In: Proceedings of 7th AIAA/USAF/NASA/ISSMO symposium on multidisciplinary analysis and optimization, St. Louis
15. Dascotte E, Strobbe J (1999) Updating finite element models using FRF correlation functions. In: Proceedings of IMAC XVII, Kissimmee
16. Lin RM, Ewins DJ (1994) Analytical model improvement using frequency response functions. Mech Syst Sign Process 8(4):437–458
17. Lammens S (1995) Frequency based validation of structural finite element models. Ph.D. thesis, Katholieke Universiteit Leuven, Leuven
18. Babuska V, Carter D, Lane S, Lacy S (2005) FRF correlation and error metrics for plant identification. In: Proceedings of 46th AIAA/ASME/ASCE/AHS/ASC structures, structural dynamics, and materials conference, Austin
19. Abrahamsson TJS, Kammer DC (2014) FEM calibration with FRF damping equalization. In: Proceedings of IMAC XXXII, Orlando
20. Craig RR Jr, Kurdila AJ (2006) Fundamentals of structural dynamics. Wiley, Hoboken
21. Kammer DC (1991) Sensor placement for on-orbit modal identification and correlation of large space structures. J Guid Control Dyn 14(2):251–259
22. Abrahamsson TJS, Bartholdsson F, Hallqvist M, Olsson KHA, Olsson M, Sällström Å (2014) Calibration and cross-validation of a car component using frequency response functions and a damping equalization technique. In: Proceedings of ISMA 2014, Leuven